euspen's 19th International Conference & Exhibition, Bilbao, ES, June 2019
www.euspen.eu

Numerical study of deformation behaviour during self-pierce riveting process

Huan Zhao[1], Li Han[2] and Xianping Liu[1]

[1] *School of Engineering, University of Warwick, Coventry CV4 7AL, UK*
[2] *Jaguar Land Rover, Coventry CV3 4LF, UK*

H.Zhao.14@warwick.ac.uk

Abstract
Self-piercing riveting (SPR) is a cold forming process, and it is one of the main connecting methods for aluminium alloy parts in automotive production. The deformation behaviours of rivet and sheets at different joining stages (clamping, piercing, flaring and tool releasing) are critical for the SPR joint quality. In order to find out the rivet and die selection rules for different stack configurations, it is necessary to explore the deformation behaviours of sheets and rivet during the riveting process. However, it is very difficult to investigate the material deformation behaviour using experimental method, because of the long testing cycle and huge numbers of SPR joints. In contrast, the finite element method (FEM) is more flexible and efficient to capture the detailed information inside the joints during the self-piercing riveting process. In this paper, a two-dimensional (2D) axisymmetric SPR simulation model for AA5754 aluminium sheets was established using commercial finite element software Simufact.Forming. Then, the deformation behaviours of the rivet and sheets in SPR joints with different top sheet thicknesses were numerically analysed.

Keywords: Self-piercing riveting, material deformation, top sheet thickness, FEM

1. Introduction

In order to meet the environmental protection requirements, lightweight materials, such as aluminium alloys and composites, have been widely used in automotive industry to reduce the fuel consumption [1]. The joining method should match the mechanical and chemical properties of the materials. Self-piercing riveting (SPR) is a cold mechanical joining technique and has many advantages compared with resistance sopt welding (RSW) [2][3][4]. Thus it has been widely used in the automative industry.

Due to the long test cycle and huge numbers of SPR joints, it is very difficult to carry out a systematical study on the deformation behaviours of the rivet and sheets using experimental tests. As an alternative, finite element method (FEM) is more flexible and efficient to capture the detailed information inside the joints during SPR process. In this study, a two-dimensional (2D) axisymmetric simulation model was established using commercial finite element (FE) software Simufact.Forming [5], and then the effects of the top sheet thickness on the deformation behaviours of the rivet and sheets were numerically analysed.

2. Finite element model

A two-dimentional (2D) axisymmetric simulation model was established in Simufact.Forming. The schematic of the SPR simulation model was shown in Figure 1. The punch, blank-holder and die were modeled as rigid bodies, while the rivet and sheets were modeled as elastic-plastic bodies.

The material of top and bottom sheets is AA5754 aluminium alloy, while the rivet is made of boron steel. The plastic stress-strain curves for AA5754 were referred to Carandente's work [5]. However, only the stress-strain curves with strain rate=1 s^{-1} were utilized in this study (shown in Figure 2). Figure 3 presents the stress-strain curve of boron steel rivet obtained from Jaguar Land Rover (JLR).

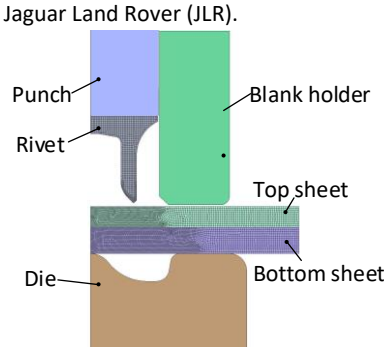

Figure 1. Schematic of the SPR simulation model

The rivet was modeled using 4-nodes Quadtree elements to distribute more elements on the edges, while the top and bottom sheets were modeled using 4-nodes Advancing Front Quad elements. The mesh size for the rivet, top sheet and bottom sheet were 0.1, 0.1 and 0.12 mm respectively. Due to the large deformation of the sheets' material during the SPR process, automatic re-meshing technique based on different re-meshing criteria was employed to avoid the severe distortion of elements. A geometrical separation method was implemented to model the blanking of the top sheet and the critical split thickness was set to 0.04mm in this simulation model.

The Columba friction law [6] was chosen to model the interactions between contacted surfaces. Inverse method was used to determine the friction coefficients between different components. The friction coefficient between the die and bottom sheet was 0.22, while firction coefficients between other contacted surfaces were 0.1.

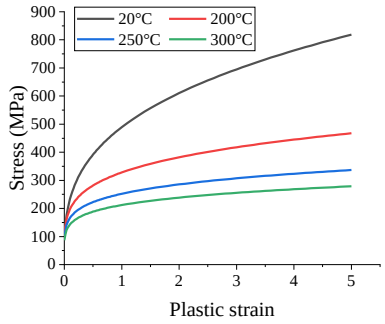

Figure 2. Stress-strain curves of AA5754 sheet (strain rate=1 s^{-1}) [5]

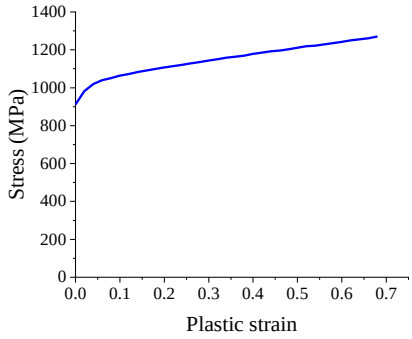

Figure 3. Stress-strain curves of boron steel rivet

3.Experiment design

In order to study the deformation behaviours of the rivet and sheets, the riveting processes of four SPR joints with different top sheet thicknesses (shown in Table 1) were simulated using the established simulation model. The punch speed used in this paper is 100mm/s, and the total punch displacement is 5.05mm.

Table 1 Parameters of SPR joints with different top sheet thicknesses.

No.	Sheet thickness		Rivet	Die		
	Top (mm)	Bottom (mm)	Length (mm)	Depth (mm)	Diameter (mm)	Pip height (mm)
1	1.0	1.5	5	1.6	9	0
2	1.2					
3	1.5					
4	2.0					

In order to evaluate the SPR joint quality and the deformation behaviours of rivet and sheets, several geometric parameters were measured from the cross-sectional profile of SPR joint as presented in Figure 4. The rivet head height (H_1), interlock (L_1) and minimum remaining thickness of the bottom sheet (T_{min}) are utilized to evaluate the joint quality. While the deformed rivet height (H_2) and deformed rivet shank radius (R_1) are used to describe the deformation degree of the rivet. In addition, the bottom sheet thickness at the rivet axis (t_1) and the bottom sheet thickness under rivet tip (t_2) were utilized to describe the deformation behaviour of bottom sheet. The distance from the left boundary of the interlock to the rivet axis (L_2) and the deformed rivet shank radius (R_1) worked together to locate the site where the interlock formed.

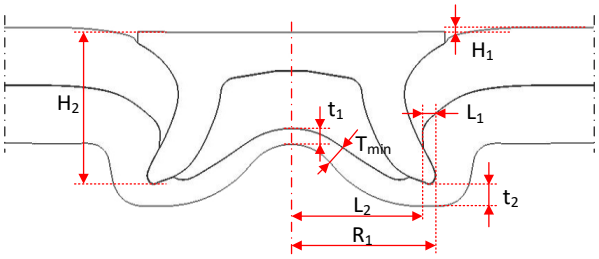

Figure 4. Geometric parameters measured on the SPR joint

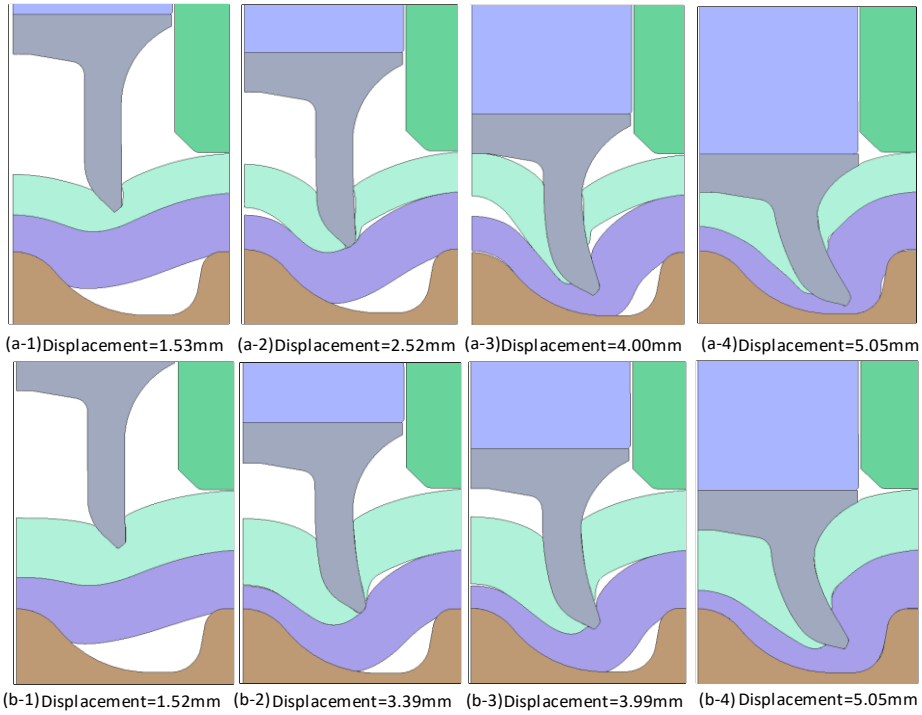

Figure 5 SPR processes with different top sheet thicknesses (a) 1.0mm; (b) 1.5mm.

4. Results and discussions

The cross-sectional geometries of SPR joints with top sheet thickness 1.0 and 1.5 mm are presented in Figure 5. The total stack thickness increased with the increment of the top sheet thickness, which led to a larger stack stiffness. By comparing the two riveting processes, it can be seen that a larger rivet displacement needed for the rivet to pierce through the top sheet increased due to the increment of the top sheet thickness (as shown in Figure 5(a-2)(b-2)). It was also found that the left part of top sheet became more difficult to deform as presented in Figure 5(a-3)(b-3). During SPR process, the left part of thin top sheet first moved downward and pressed the left part material of bottom sheet as shown in Figure 5 (a-1), then the thin top sheet material around the rivet axis move upward due to the large deformation of top sheet material under around the rivet tip. A large gap appeared between the left parts of top and bottom sheets, as shown in Figure 5 (a-2). After the top sheet was penetrated by the rivet, the left part of thin top sheet continuously deformed and moved upward until contacted with the top surface of rivet cavity, showing in Figure 5 (a-3). Then, it was pressed by the rivet head and gradually contacted with the left part of bottom sheet in Figure 5 (a-4). In contrast, the left part of thick top sheet was difficult to deform and it underwent less deformation during the whole riveting process. Therefore the gap appeared between the left parts of top and bottom sheets was much smaller than that with thin top sheet, as shown in Figure 5 (b-3), resulting in different riveted joints.

The variation of the bottom sheet thickness at the rivet axis (t_1) was illustrated in Figure 6. Point A and point B indicated the positions where the top sheets were penetrated by the rivets. It can be seen that these two curves showed very similar decreasing tendency during the riveting process, except for a little bit difference at the rightmost part of the curves. For the joint with thin top sheet, the t_1 decreased at a high rate within a very short time and then the decreasing rate gradually declined to zero before the rivet penetrating the top sheet. The value of t_1 kept constant with the increase of rivet displacement. Finally, a sharp decrease of the t_1 was observed after a small increment at the end of the riveting process. The small increase of the bottom sheet thickness at the rivet axis (t_1) was resulted by sounding material flowing (shown in Figure 5 (a-3)). For the joint with thick top sheet, the t_1 decreased within a much longer time, and then also declined to zero before the rivet penetrating the top sheet. At last, the t_1 kept constant before a slight drop at the end of the whole process without an increment. Furthermore, it was obviously that the decreasing rates of t_1 in two riveting processes were almost same at very beginning. The t_1 for thin top sheet reduced a lot not only at the beginning but also the end of the riveting process, while the reduction of t_1 for thick top sheet mainly occurred at the beginning of the rivet process, and the degree of compression is larger relatively. This difference was mainly attributed to the different deformation behaviours of top sheets.

Figure 7 illustrated the variation of rivet shank radius (R_1) in joints with different top sheet thicknesses during the riveting process. It can be found that the rivet shank started flaring along radial direction before the top sheet was penetrated in both two cases. In contrast, the rivet shank in joint with thin top sheet flared a small distance (0.075mm) along radical direction when it penetrated the top sheet, while the rivet shank in joint with thick top sheet flared a relatively large distance (0.32mm) when it penetrated the top sheet. In the SPR process, the rivet shank in joint with thick top sheet flared faster than that with thin top sheet when displacement increased from 0 to about 3mm, which may be caused by the larger resistance force applied on the inner surface of the rivet shank with a thicker top sheet. Then when the displacement was larger than 3mm, the rivet shank in joint with thick top sheet flared with a slower rate than that with thin top sheet. There are several possible reasons for this phenomenon. Firstly, the increment of the top sheet thickness would increase the contacted area between the left part of top sheet and the rivet shank, which has a negative effect on the rivet flaring along radical direction. Secondly, the left part of thicker top sheet is more difficult to be deformed, which increases the resistance force applied on the outer surface of rivet shank and prevents the rivet flaring. Thirdly, the increment of the top sheet increases the relative position between the rivet and die during the riveting process, which leads to a relatively smaller supporting force from the die and reduces the resistance force applied on the inner surface of the rivet shank. Therefore, it can be concluded that the top sheet thickness has a very significant influence on the deformation behaviour of the rivet shank during the riveting process.

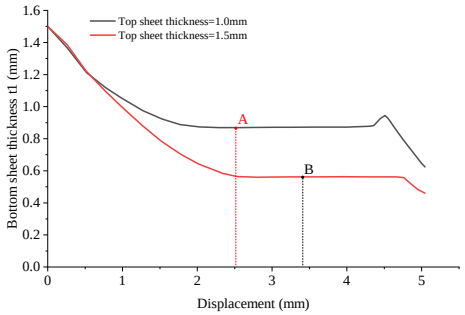

Figure 6. Bottom sheet thickness at rivet axis (t_1) with different top sheet thicknesses.

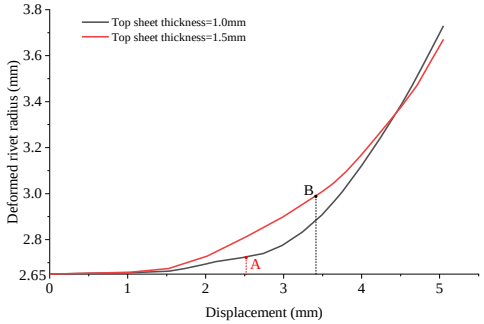

Figure 7. Deformed rivet shank radius (R_1) during SPR process with different top sheet thicknesses.

The simulation results of SPR joints with different top sheet thicknesses were illustrated in Figure 8. It could be seen that the top sheet thickness was of importance for the SPR joint feature parameters. The values of the interlock in joints with different top sheet thicknesses were shown in Figure 9 (a). With the increment of the top sheet thickness, the magnitude of interlock decreased from 0.583mm to 0.200mm. The value of interlock was directly determined by the positions of left and right boundaries of the interlock. The distances between the rivet axis and the left or right boundaries in joints with different top sheet thicknesses were illustrated in Figure 10. It can be seen that the distance between the rivet axis and left boundary increased with the increment of the top sheet thickness, while the distance between the rivet axis and right boundary decreased. With the increment of top sheet thickness, more area on the shank was wrapped by the top sheet, which made the right part material of bottom sheet be pushed along radical direction by the top sheet material rather than pierced by the

rivet shank. This led to the left boundary of interlock move along the direction far from the rivet axis. As mentioned above, the increment of top sheet also led to a relatively small deformation degree of the rivet shank, which was the main reason for the right boundary of interlock moving towards the rivet axis. Therefore, the changes of left and right boundary positions had negative effect on the formation of the interlock, and led to the decline of the interlock.

For the Tmin, it firstly increased and then decreased with the increment of the top sheet thickness as shown in Figure 9 (b). For SPR process with pip die, there are two most possible regions that the Tmin usually appears: one is around the rivet axis and another is around the rivet tip. In this study, the bottom sheet thickness at the rivet axis (t_1) and the bottom sheet thickness under rivet tip (t_2) in joints with different top sheet thicknesses were illustrated in Figure 11. The value of t_1 decreased with the increment of top sheet thickness, while the value of t_2 showed an increasing trend. These trends were resulted in above-mentioned deformation rules, namely the degree of compression for left part of bottom sheet increased, while the bottom sheet thickness under the rivet tip increased with the increase of top sheet thickness. So the Tmin appeared under the rivet tip when the top sheet was thin, while it appeared around the rivet axis when the top sheet was thick enough. Moreover, a small t_1 indicated more bottom sheet material on the left part flowed to the die cavity, which mean more bottom sheet material was filled under the rivet tip and led to a large t_2.

5. Summary

In this paper, the deformation behaviours of the rivet and sheets during the self-piercing riveting process were numerically analysed using a 2D simulation model. It was found that the top sheet thickness has an significant influence on the riveting process and the joint quality.

Acknowledgement

The authors wish to thank Jaguar Land Rover for funding and sponsoring this project.

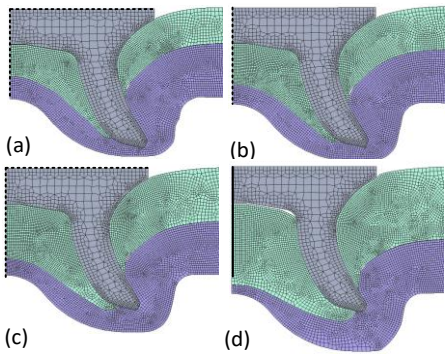

Figure 8. Cross-sectional geometries of SPR joints with different top sheet thicknesses (a) 1.0mm; (b) 1.2mm; (c) 1.5mm; (d) 2.0mm.

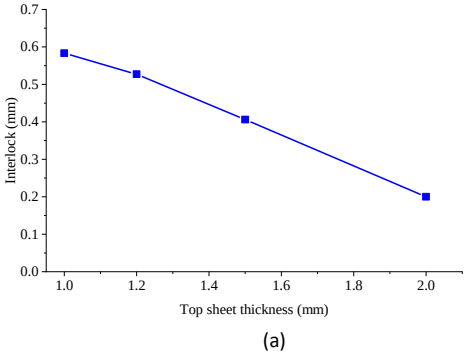

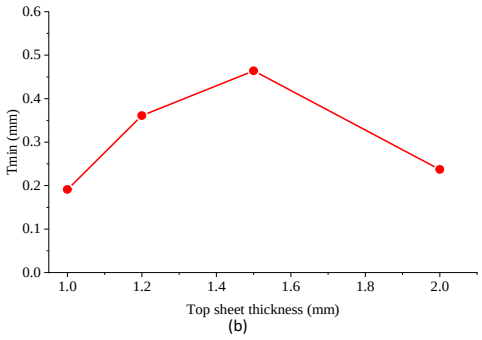

Figure 9. Predicted SPR joint feature parameters with different top sheet thicknesses: (a) interlock; (b) Tmin.

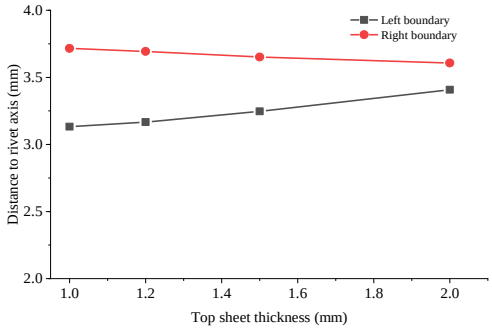

Figure 10. Interlock boundaries in joints with different top sheet thicknesses.

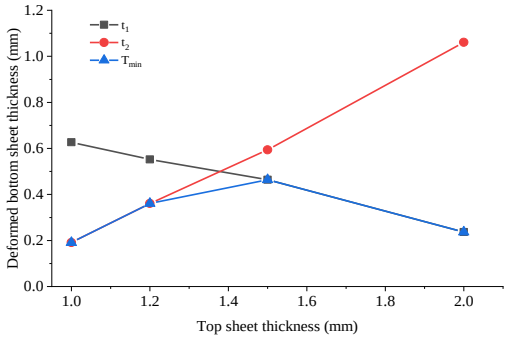

Figure 11. Deformed bottom sheet thickness in joints with different top sheet thicknesses.

References

[1] Reinhert P 2004 The new Jaguar XJ - The first all aluminium car in monocoque design, *Alum. Int. Today*, **16**, 21–24,.

[2] Han L, Chen Y. K, Chrysanthou A, and O'Sullivan J. M 2002 Self-pierce riveting - A new way for joining structures, *Am. Soc. Mech. Eng. Press. Vessel. Pip. Div. PVP*, **446**, 123-127.

[3] Han L, Young K, Hewitt R, Blundell N, and Thornton M 2009 Advanced joining technologies for aluminium assembly for the automotive industry, Key Engineering Materials, **410**, 105–116.

[4] Mortimer J 2001 Jaguar uses X350 car to pioneer use of self-piercing rivets, *Ind. Robot An Int. J.*, **28**, 192–198,.

[5] Carandente M, Dashwood R. J, Masters I. G and Han L 2016 Improvements in numerical simulation of the SPR process using a thermo-mechanical finite element analysis, *J. Mater. Process. Technol.*, **236**, 148–161.

[6] Olsson, H., Åström, K.J., De Wit, C.C., Gäfvert, M. and Lischinsky, P., 1998. Friction models and friction compensation. Eur. J. Control, **4**, 176-195.